Characterization of SEI Layers on $LiMn_2O_4$ Cathodes with *In- situ* Spectroscopic Ellipsometry

Jinglei Lei *, Lingjie Li, Robert Kostecki * [z], Rolf Muller **, Frank McLarnon **

Environmental Energy Technologies Division, Lawrence Berkeley National Laboratory,

Berkeley, California 94720, USA

* Electrochemical Society Active Member.
** Electrochemical Society Fellow.
z Email: R_Kostecki@lbl.gov

Abstract

In situ spectroscopic ellipsometry was employed to study the initial stage of SEI layer formation on thin-film $LiMn_2O_4$ electrodes. It was found that the SEI layer formed immediately upon exposure of the electrode to EC/DMC (1:1 by vol) 1.0 M $LiPF_6$ electrolyte. The SEI layer thickness then increased in proportion to a logarithmic function of elapsed time. In comparison, the SEI layer thickness on a cycled electrode increased in proportion to a linear function of the number of cycles.

Key words: Li-ion battery, $LiMnO_4$ cathode, Ellipsometry, SEI layer

Introduction

It is well known that both the anode (negative electrode) and cathode (positive electrode) in Li-ion batteries are almost covered with a passive surface layer, which is generally called the solid electrolyte interphase (SEI). Peled (1979) introduced the idea of the SEI layer on alkali and alkaline earth metals in organic electrolytes [1]. SEI layer formation has been observed for various electrode materials such as Li foil, carbon, and transition metal oxides [2-12]. The SEI layer plays a key role in the electrochemical performance and calendar life of Li-ion batteries because it prevents the electrode surface from further reacting with the electrolyte components, thereby increasing the cell impedance and decreasing its cycling efficiency [13]. Due to its important role in Li-ion batteries, a number of analytical techniques, such as X-ray photoelectron spectroscopy (XPS) [2-4, 10,11], nuclear magnetic resonance (NMR) [8], Fourier transform infrared (FTIR) spectroscopy [9-11], etc., have been employed to study the nature and formation mechanisms of the SEI layer.

Reported thicknesses of SEI layers on anodes (Li metal or carbon) have ranged from tens to hundreds of nanometers [4, 5]. Compared with the anode SEI layer, the cathode SEI layer is apparently so thin that its presence has not been confirmed until recently. Greenbaum et al. used NMR to detect a passivating layer on a $LiNi_{0.8}Co_{0.2}O_2$ cathode and concluded that it eventually led to the loss of electrical contact between active cathode particles [8]. McBreen et al. observed the formation of a SEI layer on a $LiNi_{0.85}Co_{0.15}O_2$ cathode by using X-ray absorption spectroscopy (XAS) [14]. Aurbach et al. found that a SEI layer, which consisted mainly of ROLi, $ROCO_2Li$, polycarbonates

and some salt-reduction products such as LiF, replaced the nascent Li_2CO_3 surface films on cathode particles ($LiNiO_2$ and $LiMn_2O_4$) when batteries were stored or cycled [9, 10]. Thomas et al. detected only small differences between SEI elemental compositions for cycled and stored electrodes films [11]. In these prior studies, it was necessary to store the cathodes for hundreds of hours or be charged/discharged for tens of cycles to accumulate a sufficiently thick SEI layers for *ex situ* analysis. Hence, information on the initial stage of SEI formation, which is very important to understand the SEI formation mechanism, was invariably missed.

Ellipsometry is a very powerful tool in the investigation of thin films, even at average sub-monolayer dimensions. It works by analyzing the change of both the amplitude and phase of a polarized light beam reflected from the sample surface and extracting the sample surface properties (such as the SEI layer thickness and refractive index) with suitable models. In our previous work, we have successfully applied *in situ* ellipsometry to characterize the SEI layer in carbon/EC-DMC-$LiPF_6$ [5] and Li/polymer [6] systems. In the present study, we employ spectroscope ellipsometry for the *in situ* characterization of the SEI layer on $LiMn_2O_4$ cathodes to provide more detailed insight into the cathode SEI formation process.

Experimental

Thin-film $LiMn_2O_4$ electrodes were prepared by spin-coating a homogeneous precursor solution onto well-polished Pt substrates (diameter 2.54cm) followed the same procedure reported in our previous paper [12]. There were no additives (including

binders) in the electrode; therefore possible side reactions were avoided. The crystal structure of the thin-film $LiMn_2O_4$ electrode was examined by x-ray diffraction (XRD) using a Siemens Kristalloflex D500 diffractometer, Cu Kα radiation. An integrated Raman microscopy system, LabRam, using the He-Ne laser at λ= 632.8 nm as the excitation source, was also used to confirm the crystal structure of thin-film $LiMn_2O_4$ electrode.

Electrochemical experiments were carried out in an airtight spectro-electrochemical cell, which was assembled in a He-filled glove box and then moved into ambient air for *in situ* ellipsometry measurements. Two pieces of Li foil were used as the counter and reference electrodes. The electrolyte was EC: DEC (1:1 by volume) 1 M $LiPF_6$ from EM Science. Prior to electrochemical experiments, the $LiMn_2O_4$ cathode was placed in the cell and stored in the electrolyte for 210 minutes. The cyclic voltammograms were recorded with an EG&G potentiostat model 273 at room temperature. The scanning range was 3.5 - 4.5 V (vs. Li/Li^+) and the scan rate was 1 mV/s.

Ellipsometric spectra were acquired every 2 minutes with a 44-channel Woollam ellipsometer (M-44 system) and covered the wavelength range of 292 – 609 nm. The ellipsometer beam angle of incidence was fixed at 75.0 degrees from the cathode surface normal. Before collecting ellipsometric data, the cell was carefully aligned to ensure the light reflected from the sample surface reached the exact center of the ellipsometer detector. Because the light beam reflected from the electrode surface was very weak due

to the darkness of the cathode surface, some spectral noise was observed at 292 – 340 nm and 550 – 609 nm, even though we collected 300 spectra and averaged them to obtain the finial spectrum. Hence, only the experimental spectra 389 – 550 nm were deconvoluted and reported in this paper. Both WVASE32 (a Woollam program based on a Marquardt-Levenberg algorithm) and FlexiFit (a LBNL program based on a simplex algorithm) software were used for numerical analysis of experimental data.

Results and Discussion

The structure of the fresh $LiMn_2O_4$ electrode was examined by XRD and Raman microscopy. Diffraction peaks at $2\theta = 18.9°$, 36.4°, 44.2°, and 64.1° on the XRD pattern (not shown in this paper) and Raman bands at 580 cm^{-1} and 624 cm^{-1} (also not shown), are characteristic of the $LiMn_2O_4$ spinel, demonstrating that the as-prepared $LiMn_2O_4$ materials have the spinel structure [12].

The ellipsometric spectrum of a fresh thin-film $LiMn_2O_4$ electrode in air is shown in Fig. 1. A standard 3-layer optical model (substrate – film – air) [15] shown in Fig. 2 (a), was used to deconvolute the ellipsometric data. For simplification, the roughness of the $LiMn_2O_4$ film was ignored and the $LiMn_2O_4$ film was considered as a smooth, compact homogeneous layer on top of a Pt substrate. Based on this model, the optical constants (n, k) and the thickness of the $LiMn_2O_4$ were obtained by using the deconvolution software previously referenced. The thickness of the $LiMn_2O_4$ electrode was approximately 318 nm. The ellipsometric spectrum produced by the model is also shown in Fig. 1, and is in good agreement with the experimental data.

Fig. 3 shows the experimental spectrum that was recorded 19 minutes after the electrode was exposed to the electrolyte. The ellipsometric spectrum changed dramatically after electrolyte was injected into the cell, and there are three candidate phenomena that might explain such a change. One is that the "ambient" conditions adjacent to the $LiMn_2O_4$ electrode changed from air (optical constant: n=1.000, k=0) to electrolyte (n=1.401, k=0). The other two are related to the physical and chemical changes in the electrode-electrolyte system: one is that the thickness of the $LiMn_2O_4$ electrode would decrease if some of the $LiMn_2O_4$ dissolved into the electrolyte; and the other is that a SEI layer might form on the $LiMn_2O_4$ electrode.

A predicted (i.e., calculated) spectrum that takes into account only the contribution of the electrolyte is also shown in Fig. 3; it differs from the experimental data, indicating that simply changing the ambient conditions cannot explain the apparent electrode changes. When the second possibility is also taken into account, the best predicted spectrum (not shown in Fig. 3), based on the model shown in Fig. 2(a) and an assumption of no changes in the optical constants of the $LiMn_2O_4$ electrode, still differs from the experimental data. Moreover, the fitted thickness of the $LiMn_2O_4$ electrode increased to 322 nm, which is counter to our expectation. Hence, the third possibility (spontaneous SEI formation) was taken into account, and the model shown in Fig. 2 (a) was revised to the one shown in Fig 2. (b) for deconvoluting the ellipsometric spectra of $LiMn_2O_4$ in electrolyte. The presence of the SEI layer is not unexpected, because spontaneous SEI formation on Li-ion battery cathodes has been reported. For example,

Aurbach et al. suggested that the SEI layer contained some lithium salts and polymeric alkyl carbonates formed on the surface of LiM_xO_y (M=Ni, Mn) upon storing or cycling in electrolytes such as $LiAsF_6$, $LiPF_6$, and $LiC(SO_2CF_3)_3$ [10]. In our previous paper [12], the transformation of the $LiMn_2O_4$ electrode surface into λ-MnO_2 and other products was confirmed by the Raman and surface-enhanced Raman spectroscopy (SERS) results. Thus, it seems very plausible to add a thin and uniform surface layer on the $LiMn_2O_4$ electrode when we model the $LiMn_2O_4$ electrode/electrolyte system. The new model is shown in Fig. 2 (b), and it can be used to fit the experimental data very well. The fitted spectrum is shown in Fig. 3.

With the above-described model shown in Fig. 2 (b) that takes into account spontaneous SEI formation, transient changes in both the SEI layer thickness and the $LiMn_2O_4$ electrode are calculated with the assumption that the inherent optical constants of the SEI and $LiMn_2O_4$ electrode are invariant. For $LiMn_2O_4$, the above assumption is reasonable because the $LiMn_2O_4$ electrode was not charged or discharged during its initial exposure to electrolyte. On the other hand, it is very possible that the SEI optical constants changed because its components might change with time due to chemical reactions. However, considering that the period of our experiments was short (only several hours), changes of the SEI layer chemistry and chemical rations could be ignored, at least as a first approximation. Hence, the assumption of invariable SEI optical constants may be acceptable during a short experiment period, especially at the initial stage. In addition, this assumption decreases the number of fitting parameters used in data deconvolution, which is helpful to obtain more reliable fitted results.

Figures 4 (a) and (b) show the respective changes of thickness of the SEI layer and the $LiMn_2O_4$ cathode with time. Note that spectra were not acquired during the first 19 minutes because the cell had to be mounted on the ellipsometer and realigned after being filled the electrolyte. The SEI layer thickness after 19 minutes was very close to that after 210 minutes, which implies that SEI layer formation began as soon as the electrode contacted the electrolyte and the initial SEI layer growth was rapid. The change of SEI layer thickness with time can be fitted as a logarithmic function:

$$d_{SEI} = 1.069 + 1.011 \times 10^{-1} \times \ln(t + 2.121 \times 10^{-1}) \quad [1]$$

where d_{SEI} and t respectively denote the SEI layer thickness and its contact time with the electrolyte. The change of the $LiMn_2O_4$ electrode thickness with time, which is illustrated in Fig. 4 (b), also can be fitted as a logarithmic function:

$$d_{LMO} = 3.220 \times 10^{2} - 1.825 \times \ln(t + 9.261) \quad [2]$$

in which d_{LMO} is the $LiMn_2O_4$ thickness.

Compared with the initial rapid SEI formation, the $LiMn_2O_4$ thickness decreases gradually. Before the injection of the electrolyte into the cell, the surface of the $LiMn_2O_4$ electrode was “bare” and reacted rapidly with the electrolyte. According to prior work by our group and others [12, 16, 17], possible SEI components during initial formation and growth are $Li_2Mn_2O_4$ and solvent decomposition products. Their formation can be expressed as (El. denotes the solvent):

$$Li_xMn_2O_4 + y\ Li^+ + y\ El. \rightarrow Li_{x+y}Mn_2O_4 + y\ El.^+ \quad [3]$$

The as-formed SEI layer tends to prevent the $LiMn_2O_4$ electrode from further reaction with the electrolyte, so the rate of the above reaction decreases gradually with SEI layer growth and the change of $LiMn_2O_4$ thickness therefore follows a logarithmic function. Moreover, the decrease of $LiMn_2O_4$ thickness is slightly bigger than the SEI thickness increase. For example, during the first 19 minutes, the $LiMn_2O_4$ electrode thickness decreased by about 2.7 nm while the SEI layer thickness increased by about 1.4 nm. This relationship is consistent with the disproportionation reaction of unstable Mn^{3+} leading to Mn^{2+}, which readily dissolves into solution:

$$2Mn^{3+} \rightarrow Mn^{2+} + Mn^{4+} \qquad [4]$$

After the electrode was exposed to the electrolyte for about 210 minutes, a CV scan was carried out and the results are shown in Fig. 5. Two pairs of peaks characteristic of $LiMn_2O_4$ spinel are visible, and the capacity fades during the first 4 cycles by about 3.28%, 0.78% and 0.47%, respectively.

The *in situ* ellipsometric spectra recorded during the CV experiment were deconvoluted using the model shown in Fig. 2 (b). Changes of the SEI layer parameters were detected and calculated, and here we report only the changes at 3.5 V, which correspond to the fully discharged state of $LiMn_2O_4$. At this potential, we can neglect the contribution from partially or fully charged $LiMn_2O_4$ (such as λ-MnO_2) to the electrode optical constants, which simplifies the data deconvolution process. On the other hand, there is more than 3% capacity fade during the first cycle, which arises from irreversible reactions in the cell and has some influence on the $LiMn_2O_4$ optical constants. So, first

we had to deconvolute the ellipsometric spectrum at the beginning of the second cycle to obtain the "new" optical constants of the $LiMn_2O_4$ electrode. Changes of SEI layer thickness and $LiMn_2O_4$ electrode thickness upon cycling are shown in Fig. 6(a) and Fig. 6(b), respectively. They follow two different linear functions:

$$d_{SEI} = 1.574 + 1.366 \times 10^{-2} \times n \quad [5]$$

$$d_{LMO} = 3.1212 \times 10^{2} - 3.750 \times 10^{-1} \times n \quad [6]$$

where *n* is the number of cycles.

Conclusions

In situ spectroscopic ellipsometry was employed to study the initial stage of SEI layer formation on thin-film $LiMn_2O_4$ electrodes in the EC/DMC (1:1 by vol.) 1.0 M $LiPF_6$ electrolyte. It was found that the SEI layer formed immediately and spontaneously upon exposure of the electrode to the electrolyte. The SEI layer thickness then increased in proportion to a logarithmic function of elapsed time. In comparison, the SEI layer thickness on a cycled electrode increased in proportion to a linear function of the number of cycles. The rate of $LiMn_2O_4$ electrode dissolution decreased as the SEI layer thickness increased.

Acknowledgments

This work was supported by the Assistant Secretary for Energy Efficiency and Renewable Energy, Office of FreedomCAR and Vehicle Technologies of the U.S. Department of Energy under Contract No. DE-AC03-76SF00098. The authors thank Dr. T. Richardson and Dr. K. Striebel for assistance with the measurements.

References

1. E. Peled. *J.Electrochem. Soc*., **126**, 2047 (1979).

2. A. Schechter, D. Aurbach, and H. Cohen. *Langmuir*, **15**, 3334 (1999).

3. D. Bar-tow, E. Peled and L. Burstein. *J.Electrochem. Soc*., **146**, 824 (1999).

4. K Araki and N. Sato. *J.Power Sources*, **124**, 124 (2003).

5. F. Kong, R. Kostecki, G. Nadeau, X. Song, K. Zaghib, K. Kinoshita and F. McLarnon, *J.Power Sources*, **97,** 58 (2001).

6. F. Kong, and Frank McLarnon, *J.Power Sources*. **89**, 180 (2000).

7. K-C Moeller, H. J. Santner, W. Kern, S. Yamaguchi, J. O. Besenhand, and M. Winter, *J.Power Sources*, **119-121,** 561 (2003).

8. Y.Wang, X. Guo, S. Greenbaum, J. Liu, and K. Amine. *Electrochem. Solid-State Lett.*, **4,** A68 (2001).

9. D. Aurbach, M. D. Levi, E. Levi, H. Teller, B. Markovsky, and G. Salitra, *J.Electrochem. Soc*., **145,** 3024 (1998).

10. D. Aurbach, K. Gamolsky, B. Markovsky, G. Salitra, Y. Gofer, U. Heider, R. Oesten, and M. Schmide, *J. Electrochem. Soc*., **147,** 1322 (2000).

11. T. Eriksson, A. M. Andersson, A. G. Bishop, C. Gejke, T. Gustafsson, and J. O. Thomas, *J.Electrochem. Soc.,* **149,** A69 (2002).

12. Y. Matsuo, R. Kostecki and F. McLarnon, *J.Electrochem. Soc*., **148,** A687 (2001).

13. P. Arora ,and R. E. White, *J.Electrochem. Soc*., **145,** 3647 (1998).

14. M. Balasubramanian, H. S. Lee, X. Sun, X.Q. Yang, A. R. Moodenbaugh, J. McBreen, D. A. Fischer and Z. Fu, *Electrochem. Solid-State Lett*., **5,** A22 (2002).

15. R. M. A. Azzam and N. M. Bashara, "*Ellipsometry and Polarized Light"*, North-Holland Publishing Company, 1977.

16. K. A. Striebel, E. Sakai, and E. J. Cairns, J.*Electrochem. Soc*., **149,** A61 (2002).

17. M. M. Thackeray, Y. Shao-Horn, A. J. Kahaian, K. D. Kepler, E. Skinner, J. T. Vaughey, and S. A. Hackney, *Electrochem. Solid-State Lett.,* **1**, 7 (1998).

Figure captions:

Figure 1. Ellipsometric spectra of a fresh thin-film $LiMn_2O_4$ electrode in air.

Figure 2. Optical model for deconvoluting ellipsometric spectra. (a). Without SEI layer. (b). With SEI layer.

Figure 3. Ellipsometric spectra of the thin-film $LiMn_2O_4$ electrode in electrolyte.

Figure 4. Thickness changes of SEI layer and $LiMn_2O_4$ thin-film electrode with time during storage. (a). Change of SEI layer thickness. (b). Change of $LiMn_2O_4$ thickness.

Figure 5. CV curves of $LiMn_2O_4$ thin-film electrode. The CV curves of the 2nd, 3rd and 4th cycles were overlapped.

Figure 6. Thickness changes of SEI layer and $LiMn_2O_4$ electrode with time during cycling. (a). Change of SEI layer thickness. (b). Change of $LiMn_2O_4$ electrode thickness.

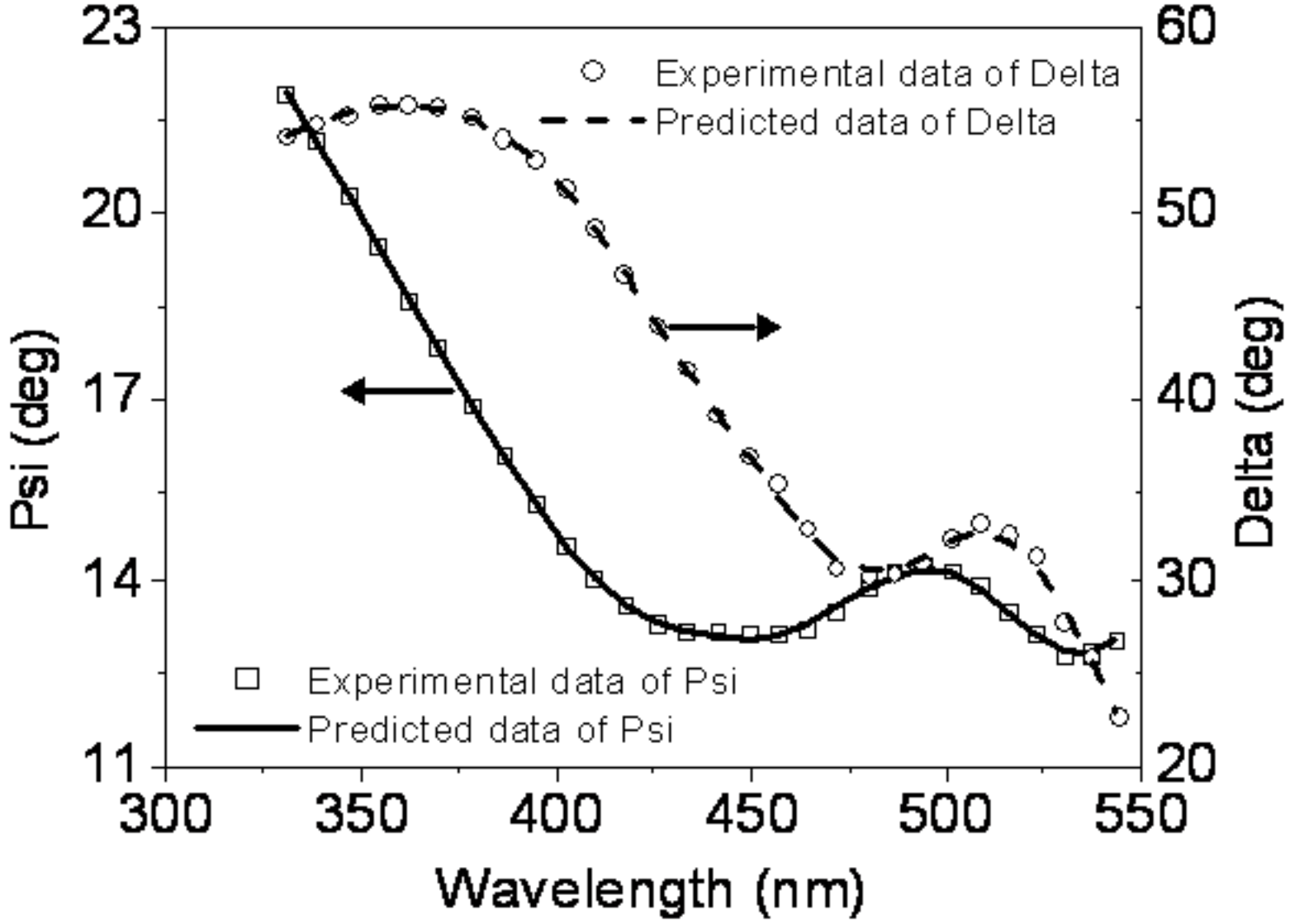
Experimental data of Delta
Predicted data of Delta
Experimental data of Psi
Predicted data of Psi
Psi (deg)
Delta (deg)
Wavelength (nm)
23
20
17
14
11
60
50
40
30
20
300
350
400
450
500
550

Figure 1

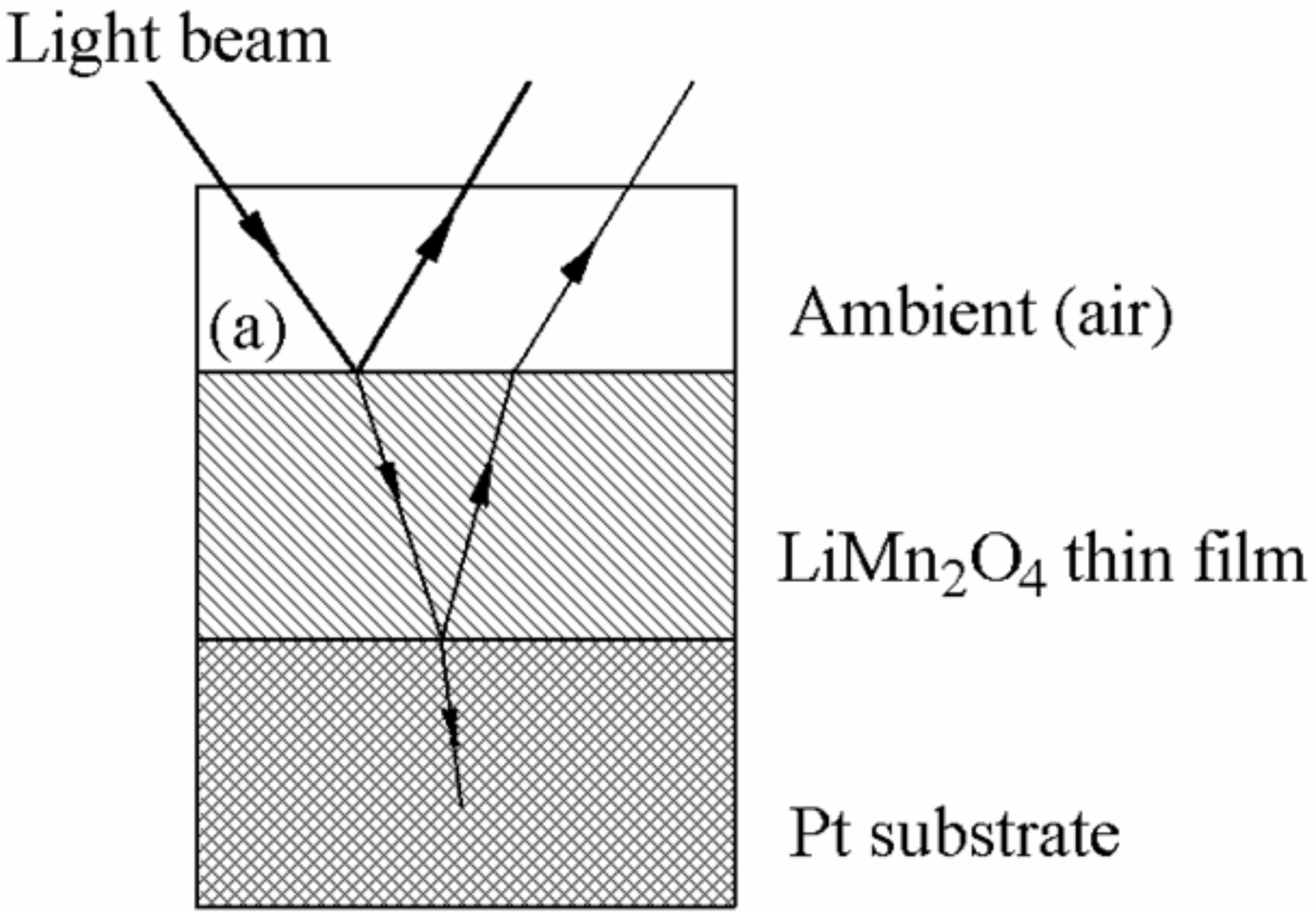

Figure 2a

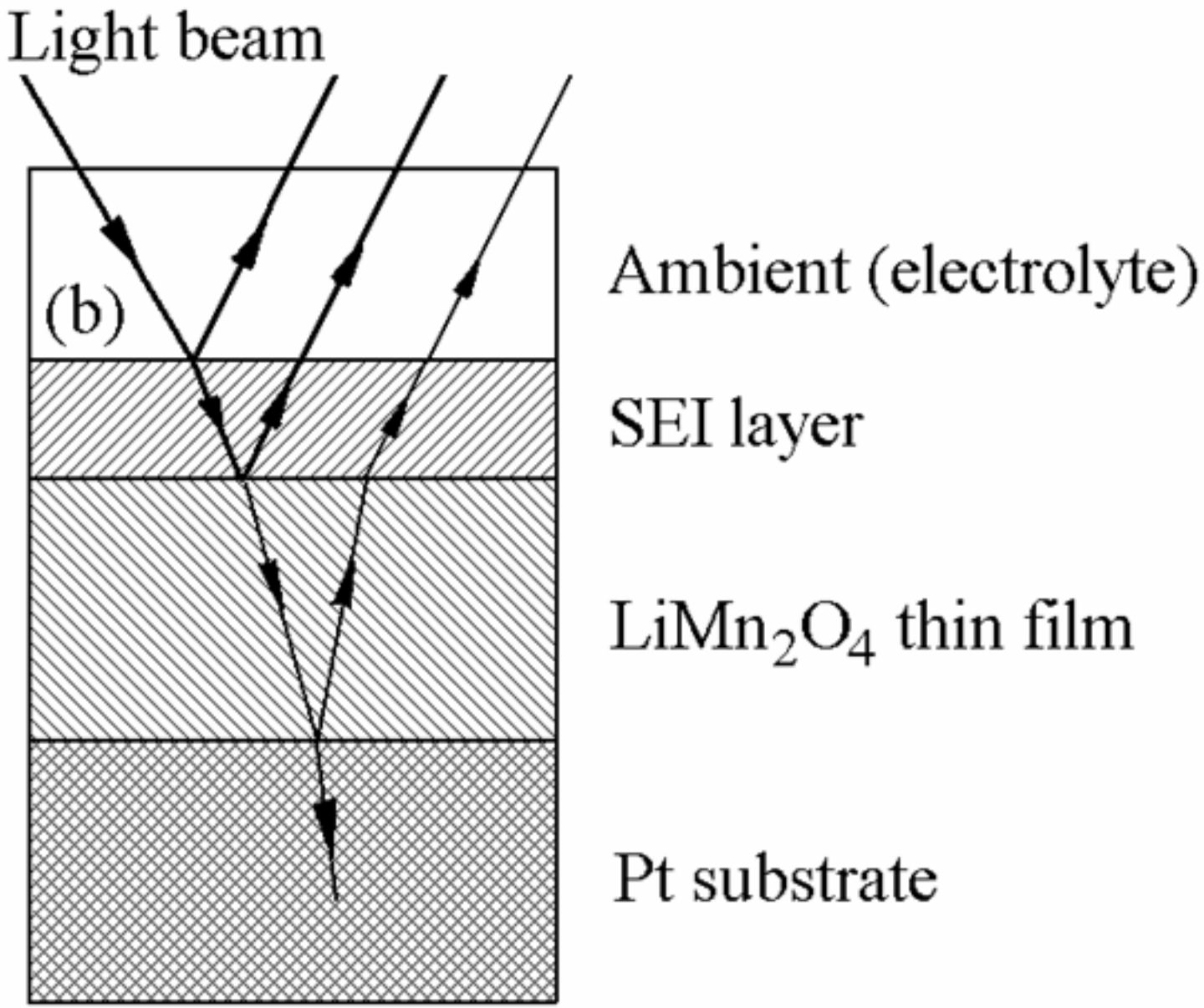
Light beam
(b)
Ambient (electrolyte)
SEI layer
$LiMn_2O_4$ thin film
Pt substrate

Figure 2b

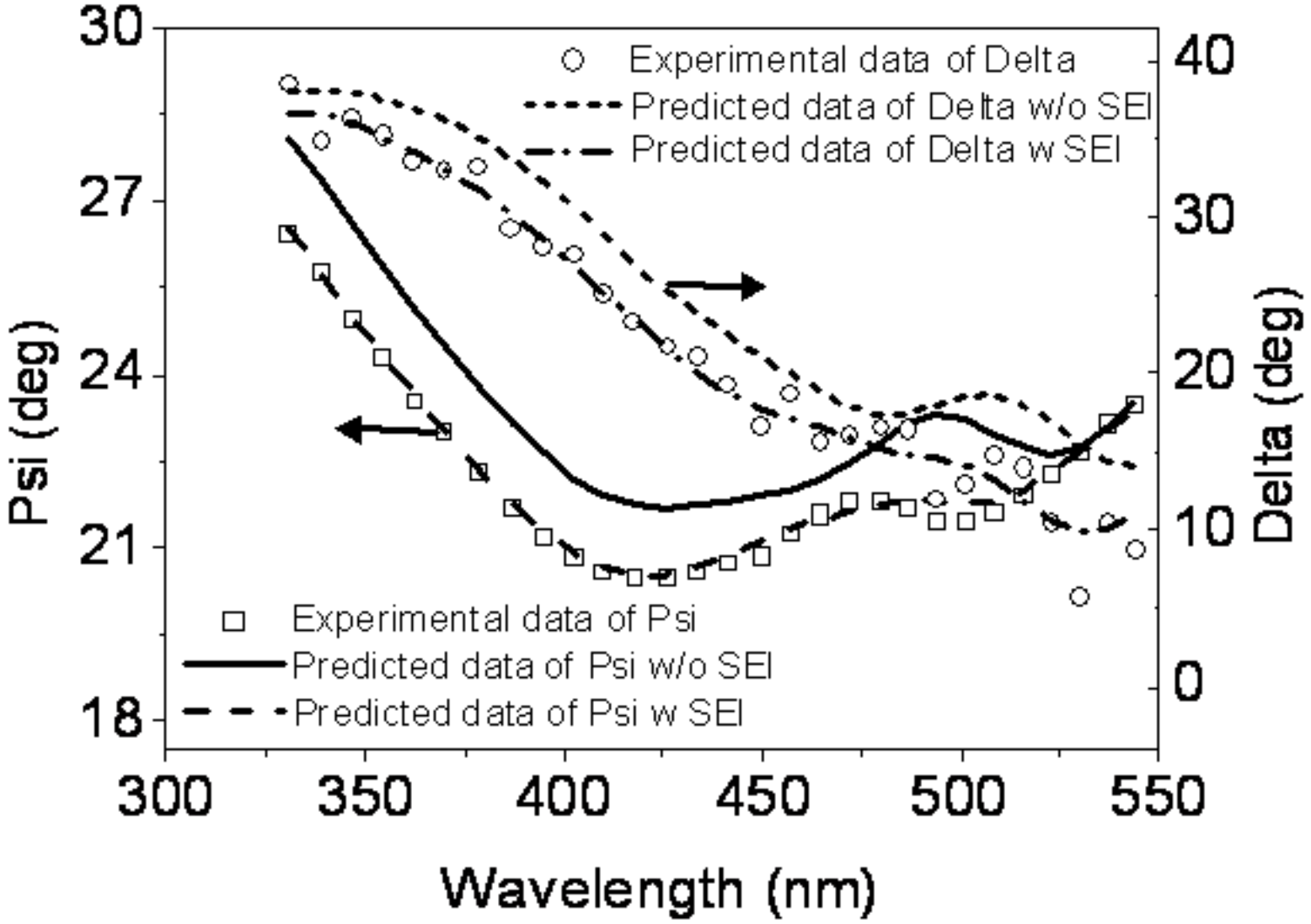
Experimental data of Delta
Predicted data of Delta w/o SEI
Predicted data of Delta w SEI
Experimental data of Psi
Predicted data of Psi w/o SEI
Predicted data of Psi w SEI
Psi (deg)
Delta (deg)
Wavelength (nm)
30
27
24
21
18
40
30
20
10
0
300
350
400
450
500
550

Figure 3

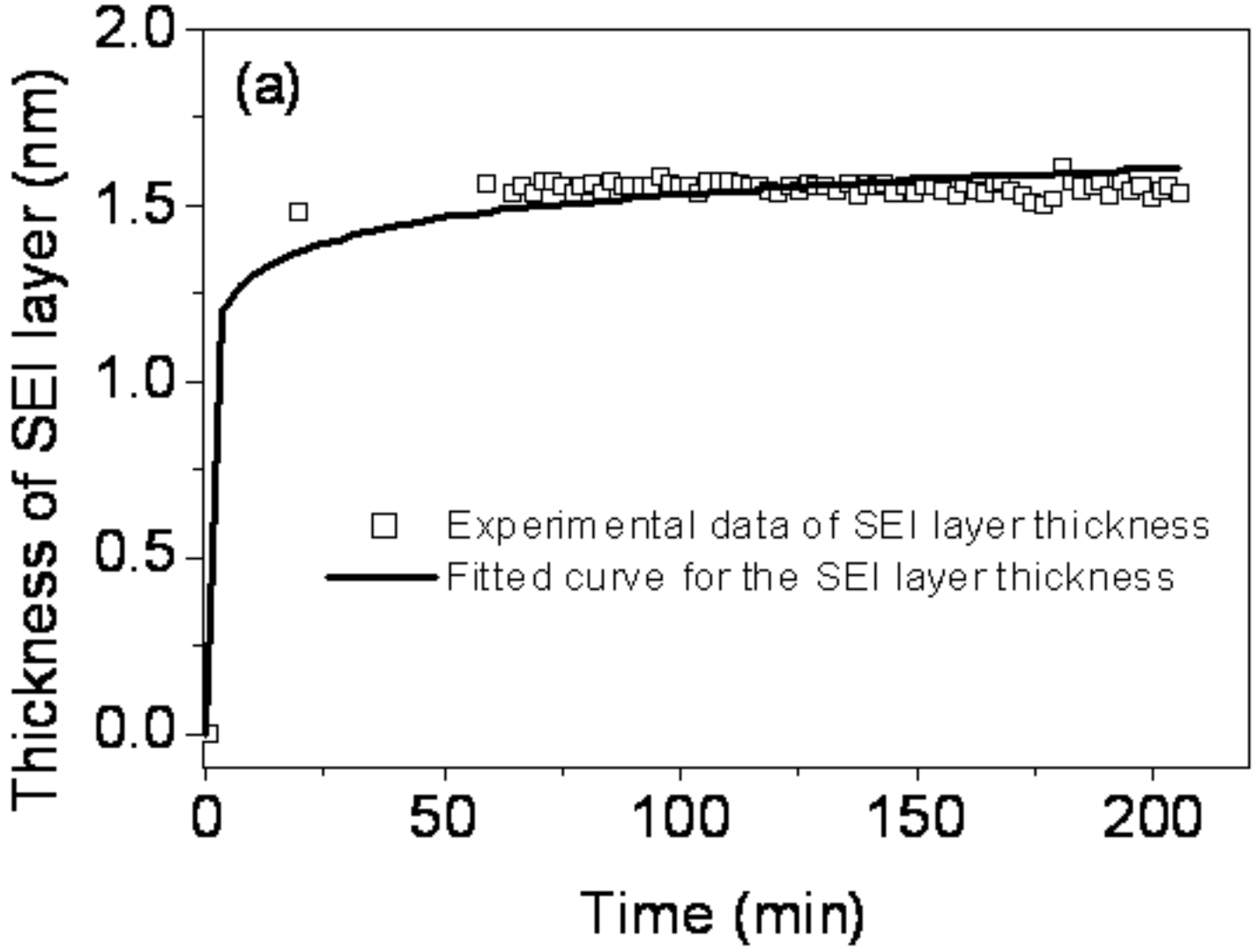
(a)
Thickness of SEI layer (nm)
2.0
1.5
1.0
0.5
0.0
0
50
100
150
200
Time (min)
Experimental data of SEI layer thickness
Fitted curve for the SEI layer thickness

Figure 4a

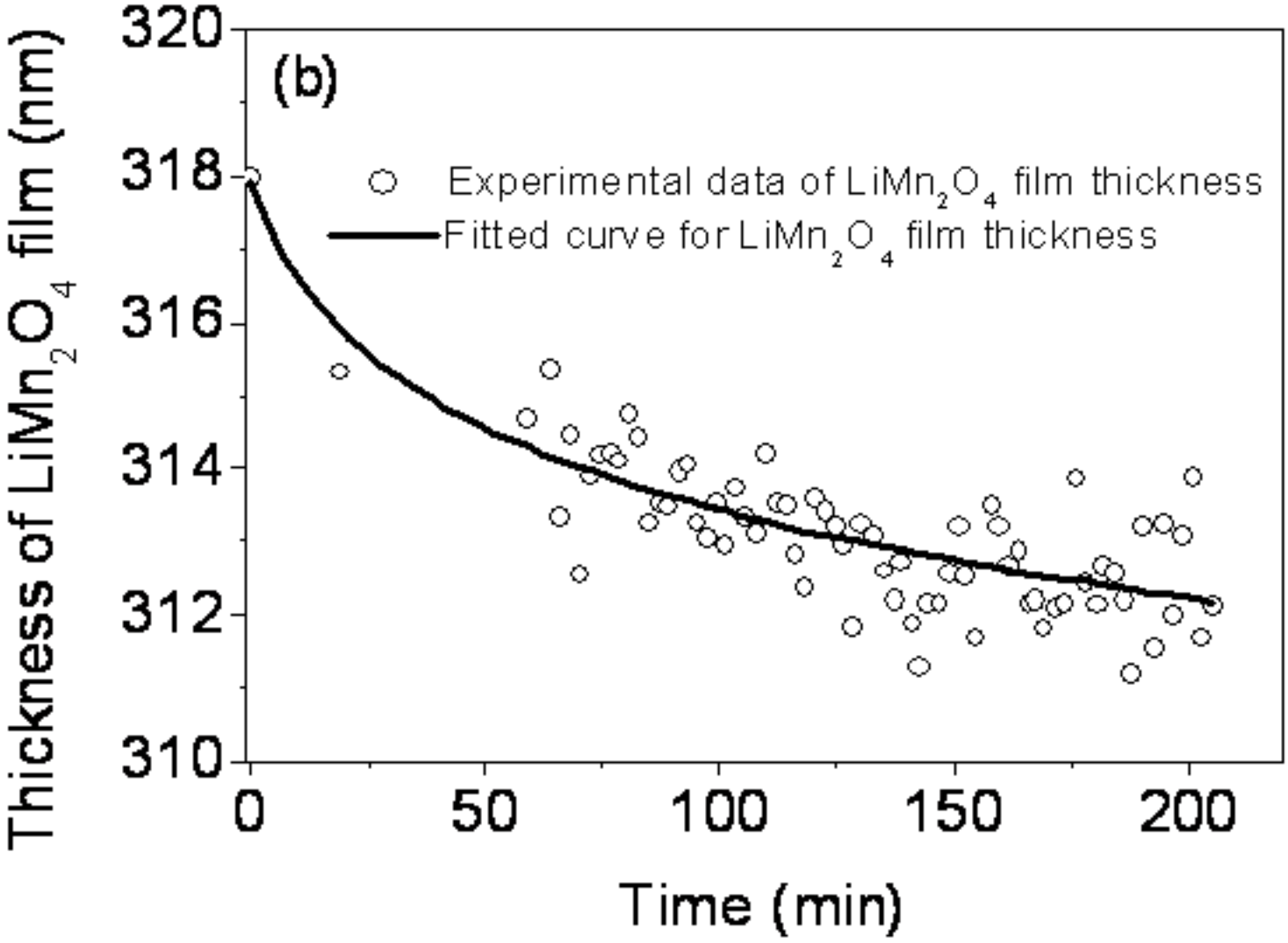
(b)
Experimental data of $LiMn_2O_4$ film thickness
Fitted curve for $LiMn_2O_4$ film thickness
Thickness of $LiMn_2O_4$ film (nm)
Time (min)
320
318
316
314
312
310
0
50
100
150
200

Figure 4b

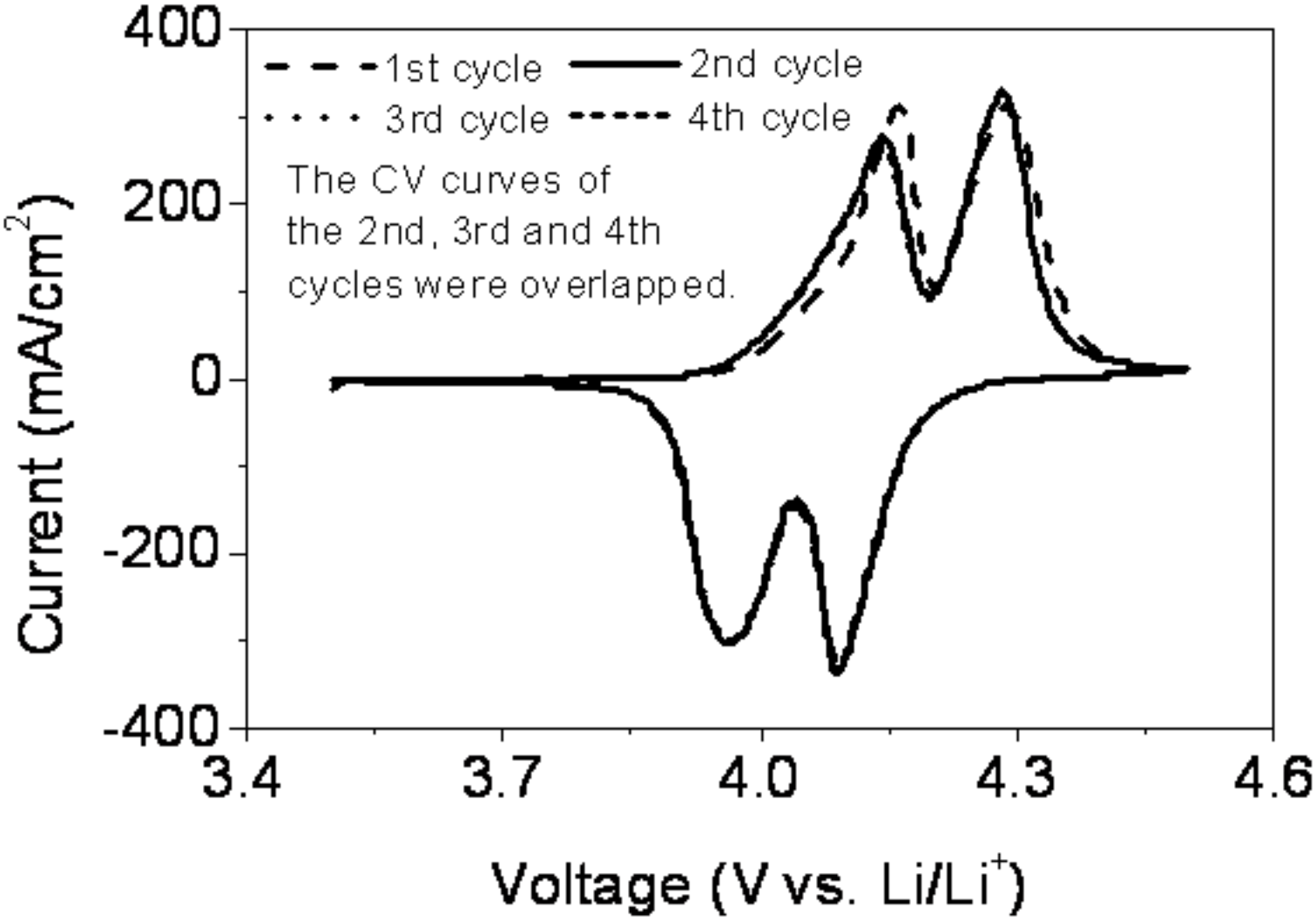
400
200
0
-200
-400
3.4
3.7
4.0
4.3
4.6
Current (mA/cm^2)
Voltage (V vs. Li/Li$^+$)
1st cycle
2nd cycle
3rd cycle
4th cycle
The CV curves of
the 2nd, 3rd and 4th
cycles were overlapped.

Figure 5

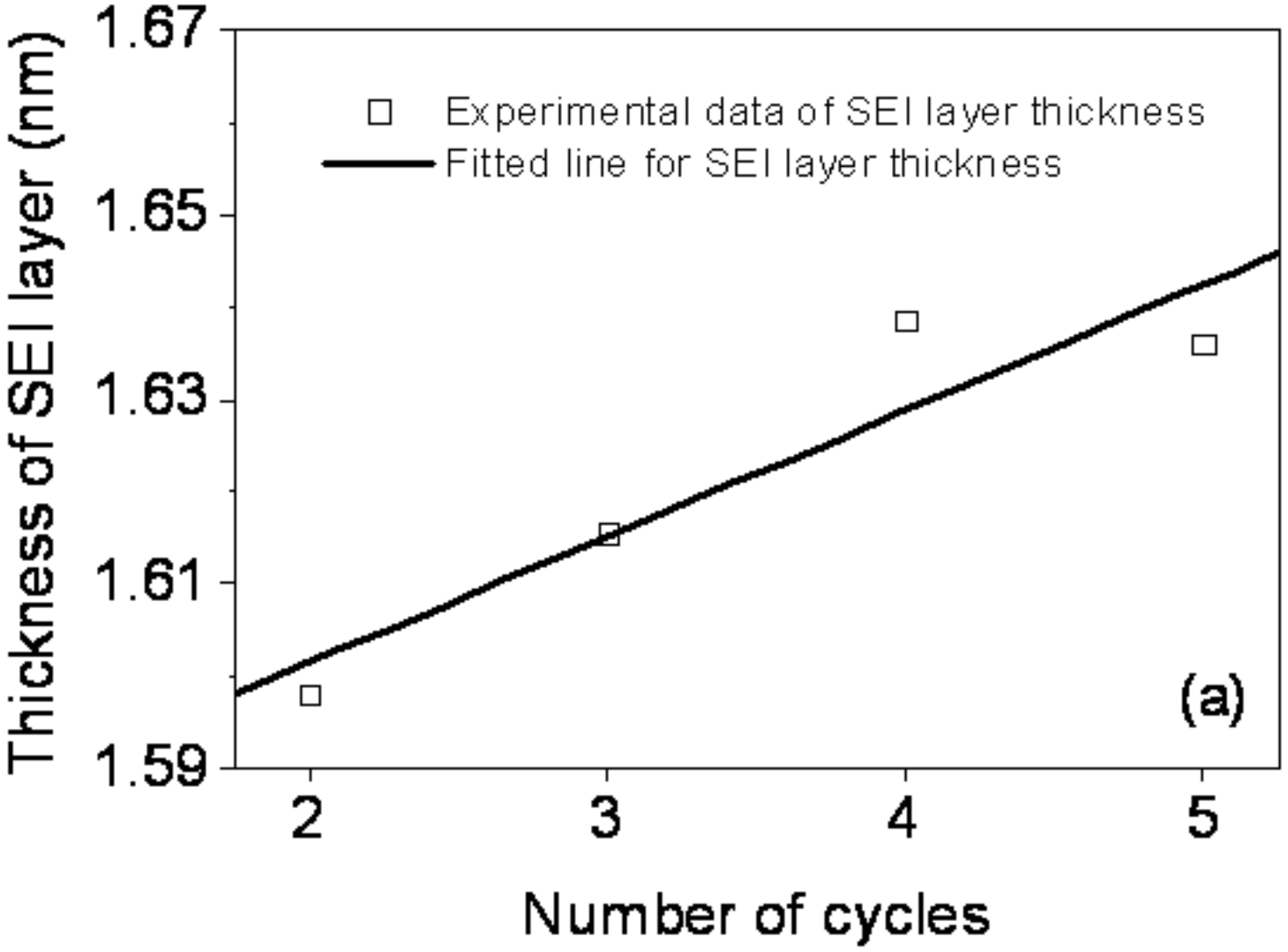
Thickness of SEI layer (nm)
1.67
1.65
1.63
1.61
1.59
2
3
4
5
Number of cycles
Experimental data of SEI layer thickness
Fitted line for SEI layer thickness
(a)

Figure 6a

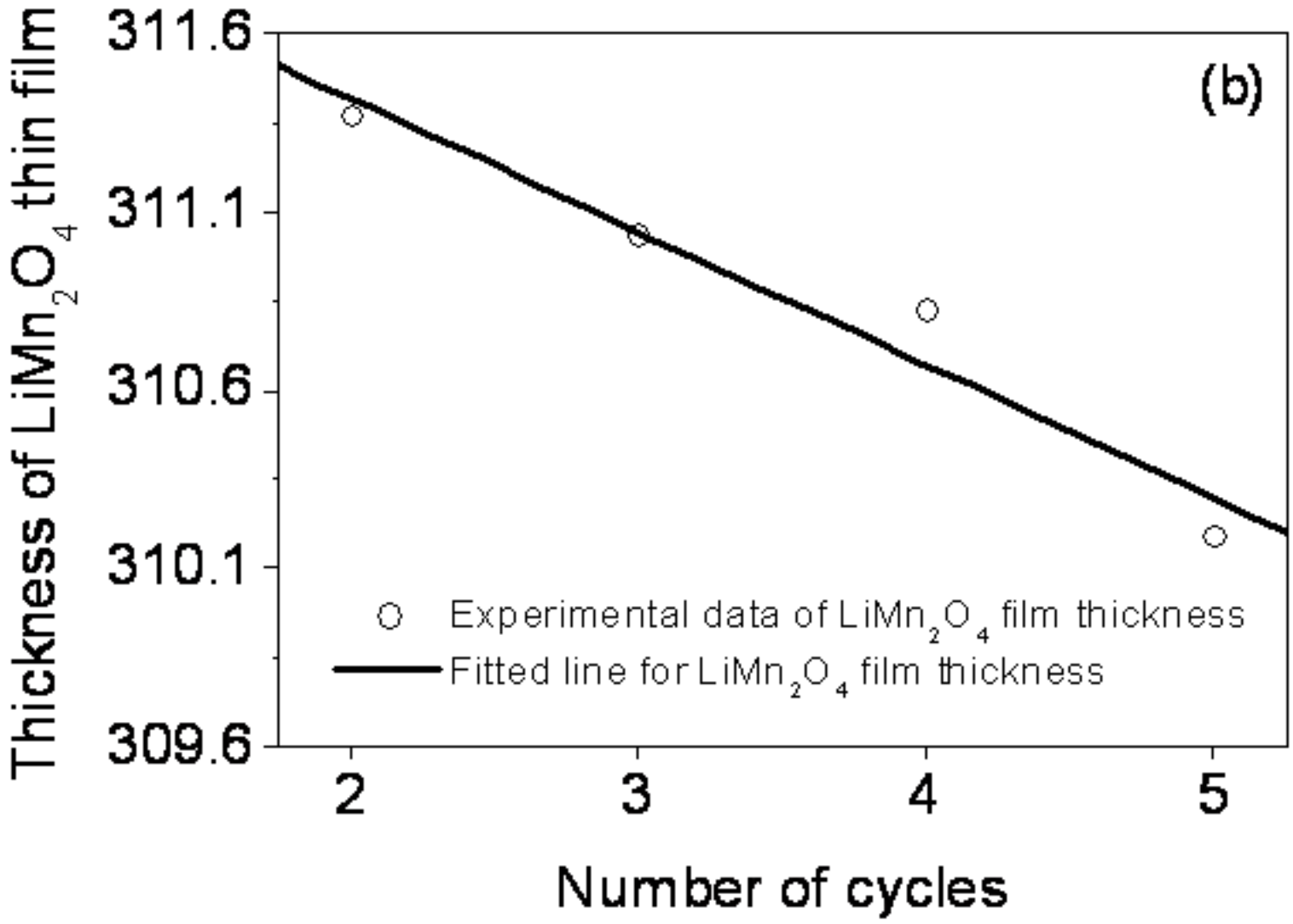
(b)
Thickness of $LiMn_2O_4$ thin film
311.6
311.1
310.6
310.1
309.6
2
3
4
5
Number of cycles
Experimental data of $LiMn_2O_4$ film thickness
Fitted line for $LiMn_2O_4$ film thickness

Figure 6b